

Osseointegration of a novel 3D porous Ti-6Al-4V implant material – Histomorphometric analysis in rabbits

Stephan Frosch¹, Gottfried Buchhorn¹, Sebastian Krohn²,
Wolfgang Lehmann¹, Karl-Heinz Frosch³, László Füzesi⁴ and Alice Frosch¹

¹Department of Trauma Surgery, Orthopaedics and Plastic Surgery, ²Department of Prosthodontics, University Medical Center Göttingen, Göttingen, ³Department of Trauma and Orthopaedic Surgery, University Medical Center Hamburg - Eppendorf, Hamburg and ⁴Department of Pathology, University Medical Center Göttingen, Göttingen, Germany

Summary. Porous structure properties are known to conduct initial and long-term stability of titanium alloy implants. This study aims to assess the histomorphometric effect of a 3-D porosity in Ti-6Al-4V implants (PI) on osseointegration in comparison to solid Ti-6Al-4V implants (SI). The PI was produced in a spaceholder method and sintering and has a pore size of mean 400 μm (50 μm to 500 μm) and mimics human trabecular bone. Pairs of PI and equal sized SI as reference were bilaterally implanted at random in the lateral femoral condyle of 16 Chinchilla-Bastard rabbits. The animals were sacrificed after 4 and 12 weeks for histomorphometric analysis. The histomorphometric evaluation confirmed a successful short-term osseointegration (4 weeks) and mid-term osseoremodeling (12 weeks) for both types of implants. The total newly formed bone area was larger for PI than for SI after 4 and 12 weeks, with the intraporous bone area being accountable for the significant difference ($p < 0.05$). A more detailed observation of bone area distribution revealed a bony accumulation in a radius of $\pm 500 \mu\text{m}$ around the implant surface after remodeling. The bone-to-implant contact (BIC) increased significantly ($p < 0.05$) from 4 to 12 weeks (PI 26.23% to 42.68%; SI 28.44% to 47.47%) for both types of implants. Due to different surface properties, however, PI had a significant ($p < 0.05$) larger absolute osseous contact (mm) to the implant circumference compared to the SI (4 weeks: 7.46 mm vs 5.72 mm; 12 weeks: 11.57 mm vs 9.52 mm [PI vs. SI]). The regional influences (trabecular vs. cortical) on bone formation and the intraporous distribution were also presented. Conclusively, the

porous structure and surface properties of PI enable a successful and regular osseointegration and enhance the bony fixation compared to solid implants under experimental conditions.

Key words: Porous Titanium Implants, Osseointegration, Bone Remodeling, Histology, Bone-Implant Contact (BIC)

Introduction

Titanium and its alloys are frequently used in orthopedics (Ti alloys) and as oral implants (cp titanium) with very good long term clinical results (Wennerberg et al., 2018). Porous structure properties may even enhance osteoconductive and osteoinductive abilities, support biological anchorage and facilitate a higher bone-implant contact (BIC) at the surface compared to solid implants (Rosa et al., 2009; Vasconcellos et al., 2010; Kim et al., 2013; Bencharit et al., 2014). In the present histomorphometric study, we investigate the bone response of an open-porous Ti-6Al-4V implant (PI) that exhibited a superior biomechanical osseous fixation compared to a solid control group in a previous study (Frosch et al., 2020). The PI was produced in a spaceholder method with a porosity of 49%. Compacting of the alloy/space holder mixture creates bridges and confluences between the paraformaldehyde spheres. As a result, differently shaped pores with a mean size of 400 μm (50 to 500 μm) were formed during sintering, which correspond to most of the proposed size ratios for optimal implant stabilization (Itala et al., 2001; Frosch et al., 2002, 2004; Karageorgiou and Kaplan, 2005; Jones et al., 2007; Xue et al., 2007; Vasconcellos et al., 2010).

Abbreviations. PI, porous implant; SI, solid implant; BIC, bone-to-implant contact; ROI, region of interest

Corresponding Author: Dr. Stephan Frosch, Department of Trauma Surgery, Orthopedics and Plastic Surgery, University Medical Center Göttingen, Robert-Koch-Straße 40, 37075 Göttingen, Germany. e-mail: Stephan.Frosch@med.uni-goettingen.de
DOI: 10.14670/HH-18-342



Macro- and microstructure mimic human trabecular bone which possibly enhances the implant stabilizing bone response of the material (Hartmann, 2012; Gittens et al., 2014). Furthermore, targeted variation of the spaceholder methods enables an adjustment of the porous structure properties according to the desired application (Hartmann, 2012). Biomechanical arrangements (e.g. push-out tests) only cover the mechanical aspect of the bony integration, whereas bone histomorphometry is regarded as the gold standard technique to quantify bone healing and remodeling (Moreira and Dempster, 2020). The aim of the present animal study was to analyze the histomorphometric findings on osseointegration of a 3-D Ti-6Al-4V PI in comparison with a conventional solid Ti-6Al-4V implant (SI) of the same size. Attention was also paid to the cortical vs. trabecular positions of the implant within the distal femur, a detailed representation of bone area distribution as well as the time course of osseointegration from short-term osseointegration after 4 weeks to mid-term osseointegration after 12 weeks.

Materials and methods

Implant materials

The SI and PI were made of Ti-6Al-4V material (ISO 5832-3 and ASTM F136) and had the same geometry in order to enable a comparison and a uniform implantation process (Fig. 1). The hollow cylinders had a height of 7.0 mm and a diameter of 5.6 mm with a central 2.0 mm drill channel. The PI were manufactured in a basic space-holder process (Fraunhofer Institute for Manufacturing Technology and Advanced Materials [IFAM], Bremen, Germany) and based on the work of Bram, Bobyn and Rausch (Bobyn et al., 1980; Rausch et al., 2000; Bram et al., 2004; Hartmann, 2012; Bram, 2013). The average pore size of 400 μm was established by sieving the paraformaldehyde spheres using an analytic sieve shaker (Vibratory Sieve Shaker, ISO 9001, Retsch Company, Haan, Germany). The mixing ratio of the titanium granules (powder fraction of 22 μm to 45 μm) to the quantity of spacer beads had to be 498.38 g to

189.75 g in order to achieve a porosity of 49%. Sintered blocks (for PI) were turned to the appropriate shape with no further surface treatment. The SI samples were turned to the given diameter and the surface was grit blasted in a standard procedure using a corundum with a grain size of 1000 μm to roughen the surface.

Animal experiment

All aspects related to the care and treatment of the animals were approved by local and federal authorities (LAVES, 28. 04. 2010, AZ 33.14-42502-04-10/0059). 16 female rabbits (Chinchilla-Bastard, Charles River GmbH, Sulzfeld, Germany) with an age of 12 to 14 weeks and a body weight not under 3 kg were included in the study, because their growth plates are almost closed and growth disorders are not to be expected in the course of the experiment (Masoud et al., 1986; Kaweblum et al., 1994). We have paid attention to a standard implantation process based on anatomical landmarks in order to exclude penetration of the implant into the patellar groove, cartilage area of the condyles or the dorsal cortex. Postoperative x-rays were performed in all animals to exclude fractures and incorrect positioning of the implant. The species-appropriate, pain-free behavior and physiological movement of the animals were regularly monitored by a veterinarian. Animals were kept in boxes (5 rabbits/2.5 m² box) on straw with standard pellet diet, hay and water ad libitum and body weight was measured every two weeks. Two animals were excluded (one from evaluation due to lack of press-fit (instrumentation problem), one sacrificed due to deep infection after bite wound).

The implant types were randomly distributed to the lateral femoral condyles of the animal bilaterally (Figs. 2, 3). Animals received preliminary i. m. anesthesia 0.3 ml (10 mg) Xylazin and 0.5 ml/kg Ketanest. The lateral knees were clean shaven, the skin was disinfected and covered sterile. Attention was paid to sterile work during operation. Continuous infusion of general anesthesia (5 ml Xylazin + 5ml Ketanest + 40 ml NaCl at 1.7 ml/kg/h) was established using an ear vein. Skin incision over the

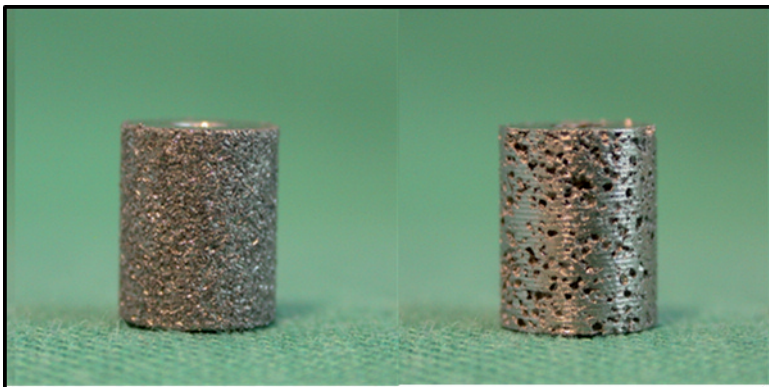


Fig. 1. Solid, blasted (left) and porous (right) Ti-6Al-4V implants.

Histomorphometry of osseointegration of novel 3D porous Ti-6Al-4V titanium implants

lateral femoral condyle and exposure of bone proximally of the growth plate allowed preparation of a cylindrical bore. A bediamonded hollow grinder (Fa. Articommed,

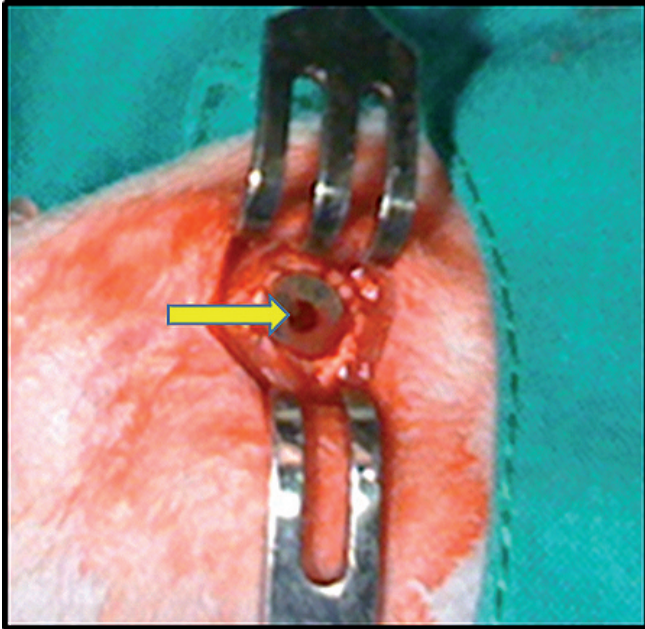


Fig. 2. Surgical site with placement of the implant in the lateral condyle of the rabbit. The lateral outer surface of the implant is flush with the cortex. The longitudinal 2.0 mm drill channel can be seen in the center of the implant (arrow).

Schlüchtern, Germany) with an outer diameter of 5.4 mm was used to reach a depth of 7 mm. Permanent cooling with physiologic saline was applied. The central bone block was extracted and the bottom of the bore was leveled. The implant was carefully centered and press-fit impacted until the lateral implant side was at best possible plane with the cortical bone (Fig 2). Wound closure in layers was followed by an intracutaneous seam and skin surface disinfection. An antibiotic (0.5 ml Penstrep) was given perioperative once and analgesic (Rimadyl 0.1 ml/kg) the following 3 days.

The animals were randomized into two groups and sacrificed after 4 and 12 weeks, respectively. The time intervals have been chosen to be able to analyze the initial osseohaling (4 weeks) and the completion of the remodeling phase (12 weeks).

The implants were left in the bone bed and removed with the entire femur. The attached soft tissue was carefully prepared. After using the combined thin-section technique and hard-cutting technique, the preparations were embedded with the cold-curing polymethyl methacrylate medium "Technovit® 9100" (Co. Heraeus Kulzer, Wehrheim, Germany). The saw microtome SP1600 (Leica Mikrosysteme Vertriebs GmbH, Bensheim, Germany) was used to cut the preparations. It was important to achieve a cut exactly perpendicular to the axis of symmetry of the implant without any angular deviation in order to ensure an accurate axis-appropriate thin-ground process. Therefore, we provided the implant with a central boring with a diameter of 2 mm that strictly follows the longitudinal axis of the implant (Figs. 2, 3). A close

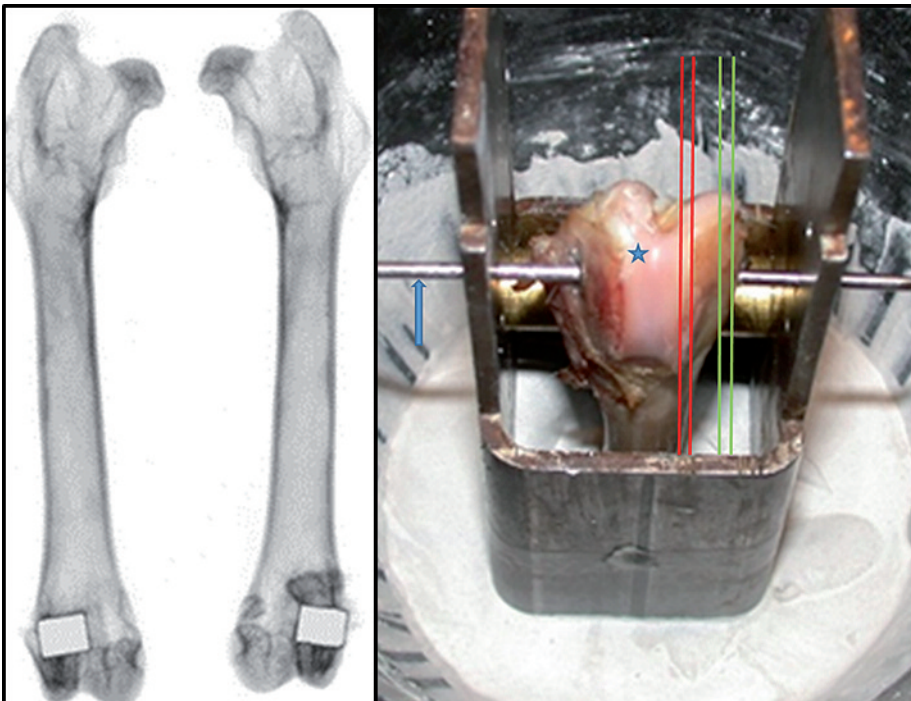


Fig. 3. Left: X-rays of the right and left femur of a rabbit. Randomized distribution of a SI and PI to the lateral condyle, 4 weeks after implantation. Right: The distal femur (star) covered with gypsum and centered in the sawing jig. The exact alignment to create the vertical cutting plane was ensured via the spike wire (arrow). This way, two cortical sections (green lines) and two trabecular sections (red lines) were placed exactly perpendicular to the longitudinal axis of the implant.

fitting spike, which was inserted into the central boring of the implant, was predefined clamped in the sawing jig (Exact Sectioning System, Messner, Oststeinbek, Germany) so that an exactly perpendicular cutting plane was created to the longitudinal axis of the implant (Fig. 3). Four sectional planes were performed along the longitudinal axis of the implant to quantify the osseointegration according to the anatomical position of the implant bed: section 1+2 for cortical cutting plane and section 3+4 for trabecular one (Figs. 3, 4).

The tissue slices should reproducibly show a circular projection of the implant cross section. After grinding and polishing, the final thickness of the preparations was 25 μm .

Histomorphometry

Histological staining was performed using the Smith and Karagianes method (Smith and Karagianes, 1974). The polished specimens were pretreated with methylene blue and then stained with alizarin red (Dahl, 1952). The digitization of the histological sections was carried out by a fully automated microscope (Axiovert 200M, Carl Zeiss, Oberkochen, Germany) connected to

a digital camera (Axiocam, Carl Zeiss, Oberkochen, Germany). The morphometry was performed using an image editing program (Adobe Photoshop® Elements 7). In addition to the sections (1-4) along the longitudinal axis, six regions of interest (ROI) were defined along the transverse axis of the implant in order to perform a three-dimensional characterization of the bone area (Fig. 5). With the help of the image processing program, concentric circles around the transverse axis of the implants with a respective radial distance of 500 μm were projected into the digitized histological sections. The area between the concentric circles were allocated to a total of 6 ROIs, which enabled a precise measurement of the newly formed bone area according to the distribution around (PI and SI) and within the implant pores (PI) (Fig. 5). The BIC was calculated with the image procession program by marking the circumferential surface line for each section image.

Interobserver variability

In order to validate the accuracy and sensitivity of the histomorphometric examination methods, three

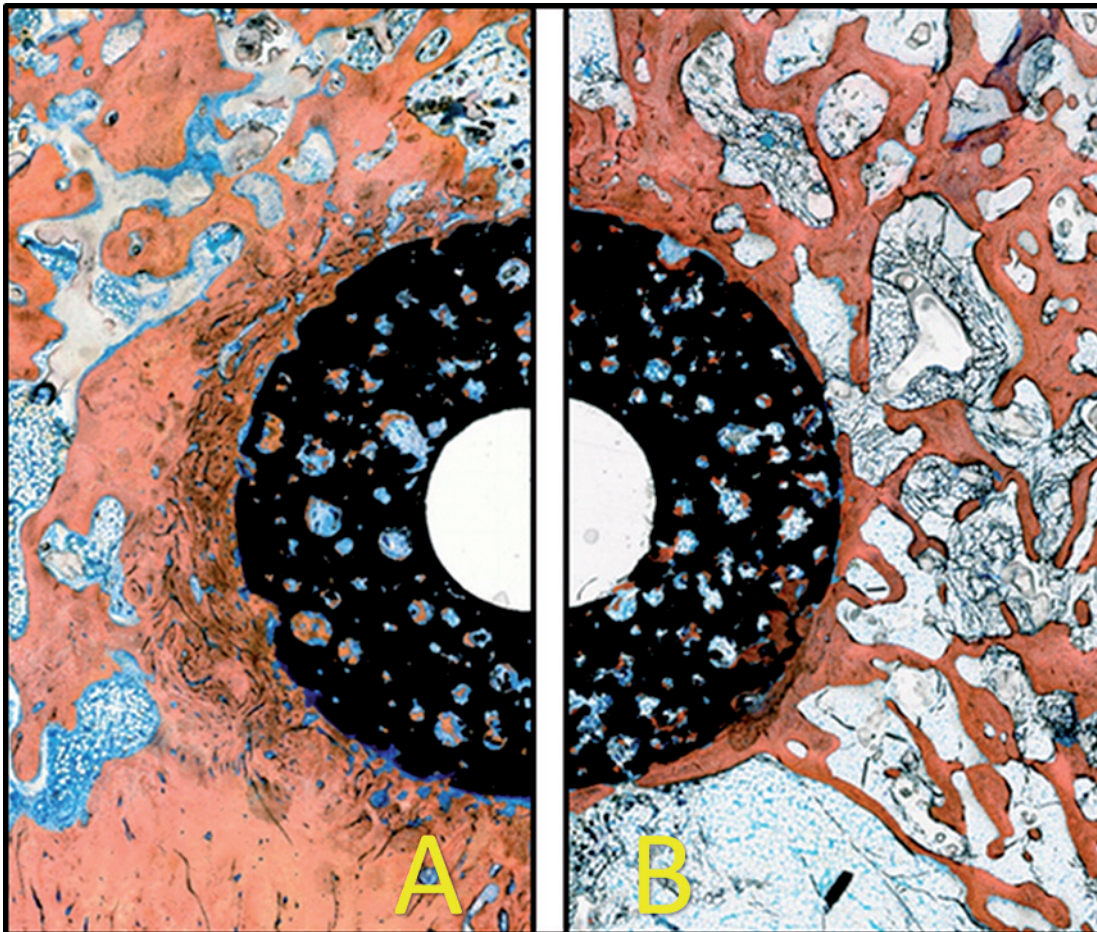


Fig. 4. Porous implant according to the anatomical position, 4 weeks after implantation: cortical section (A); trabecular section (B). Stained with methylene blue - alizarin red. x 20.

Histomorphometry of osseointegration of novel 3D porous Ti-6Al-4V titanium implants

different examiners (AF, SF, SK) carried out the histomorphometric measurements. The values of the investigators AF and SF did not differ significantly and formed the statistical basis of the present work as combined average values. The combined values of the examiners AF and SF were compared again with the values of the examiner SK without significant differences being shown.

Statistics

The distribution of every parameter was described by its mean, standard deviation and visualized separately for implant (PI vs. SI), weeks (4 vs. 12) and ROI. The effect of implant (SI vs. PI) in cortical and trabecular position and elapse time (4 vs. 12 weeks) were studied within each ROI by analysis of variance (ANOVA). Kendall's correlation coefficient was determined between cutting sections and bone area within each implant and month. In case of multiple testing situation, raw p-values were adjusted by the method of Bonferroni-Holm. The significance level was set to $\alpha=5\%$ for all statistical tests. All analyses of variance for repeated measures were performed with the statistical software R (version 3.0.2, www.r-project.org) using the R-package 'lme4' and 'lmerTest'.

Results

The mean implant circumference of the raw implants was significantly larger ($p<0.05$) for the PI (28.44 ± 3.71 mm) than for the SI (20.08 ± 0.25 mm).

The BIC (%) showed no significant difference between PI and SI, but a significant increase has been observed from 4 to 12 weeks for both implant types (Table 1). However, if the almost 42% larger implant circumference of the PI (28.44 mm) compared to the SI (20.08 mm) is taken into account, the total bone contact in mm with the implant circumference is significantly larger to PI than to SI after 4 and 12 weeks (Table 1). When comparing the cortical (sections 1 and 2) and the

Table 1. Mean (\pm standard deviation) of BIC (%) and direct osseous contact (mm) to the implant circumference in time (section 1-4).

Weeks	PI	SI	p-value
4	26.23% (± 9.07)	28.44% (± 10.89)	0.6054
	7.46 mm (± 2.58)	5.72 mm (± 2.19)	<0.05
12	42.68% (± 8.83)	47.47% (± 7.47)	0.2486
	11.96 mm (± 2.51)	9.52 mm (± 1.5)	<0.05
p-value (4 vs. 12)	<0.05 (% , mm)	<0.05 (% , mm)	

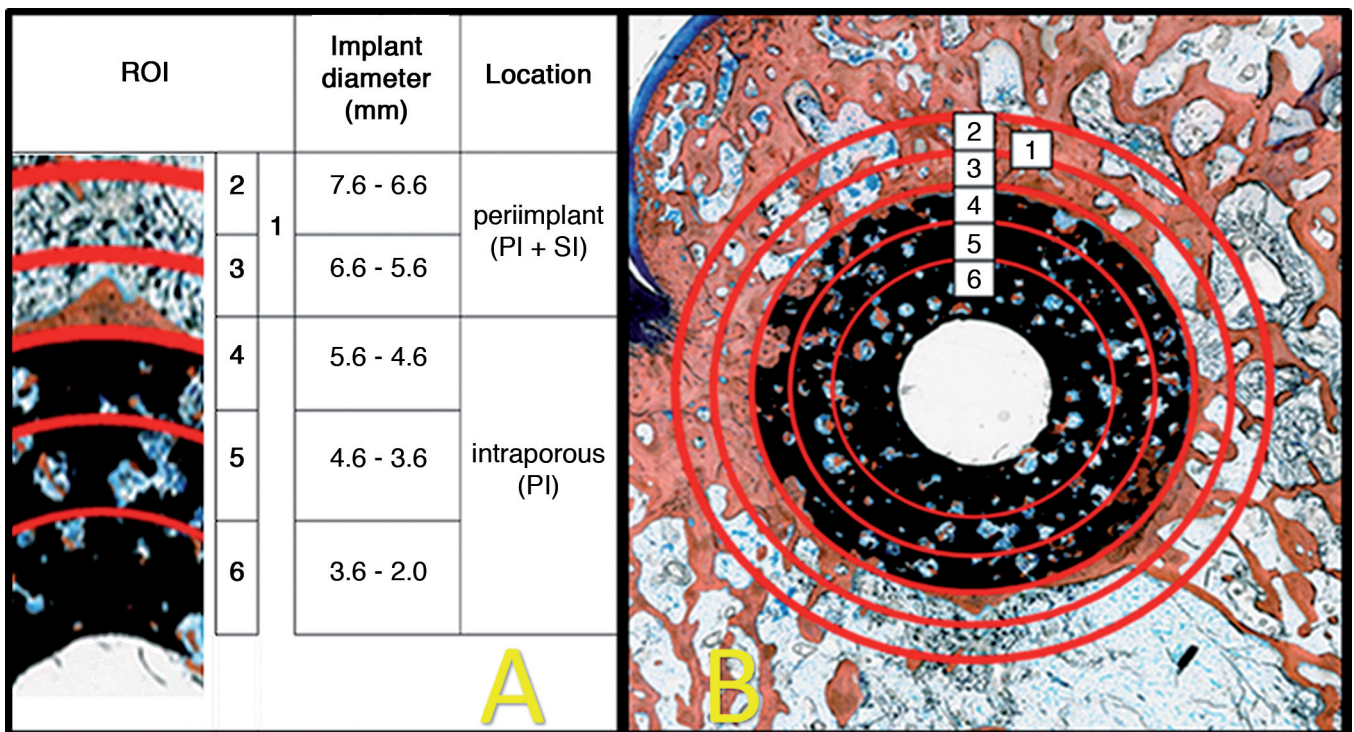


Fig. 5. A. Axial concentric ring circles formed corresponding ring areas, which were each assigned to a region of interest (ROI) 1-6. **B.** Local distribution of ROI 1-6. The peri-implant ROI 1 was divided into ROI 2 and 3 in order to be able to differentiate the peri-implant bone distribution more precisely during remodeling.

Histomorphometry of osseointegration of novel 3D porous Ti-6Al-4V titanium implants

trabecular (sections 3 and 4) bone contact to the implant circumference (in mm), no significant difference was found in the separate assessment for PI and SI either after 4 or 12 weeks (Table 2). In both regions, the direct bone contact with the implant circumference was larger for PI than for SI at 4 and 12 weeks (Table 2).

The newly formed bone area around the implants (ROI 1) of SI and PI did not differ significantly (Table

3). However, the total bone area including the intraporous portion of PI (ROI 4-6), was significantly larger in PI compared to SI after 4 and 12 weeks, respectively (Table 3). Overall, the bone area in total decreased from 4 to 12 weeks for both types of implants, but without any significant difference (Table 4). Considering this process in more detail, the bone area further away from the implant (ROI 2) decreases significantly for SI from 4 to 12 weeks and not significantly for PI, while the bone area next to the implant (ROI 3) remains similar for SI and PI (Table 5). In the pores of PI (ROI 4-6), the amount of newly formed, mineralized bone decreased from peripheral to central at 4 and 12 weeks, with a significant decrease from ROI 4 to ROI 5 (Table 6). A significant time effect (4 to 12 weeks) was not detectable. In contrast to the cortical sections, in which both types of implants were circular and largely walled by bone tissue, the trabecular sections showed a regular metaphyseal structure, with the bone having larger, bone-free recesses peri-implant that were filled with fat tissue at 4 and 12 weeks. The

Table 2. Mean (± standard deviation) of osseous contact to implant circumference (mm), time and region.

weeks	Implant	Cortical (section 1+2)	Trabecular (section 3+4)	p-value
4	PI	8.44±2.74 mm	6.79±2.39 mm	0.0773
	SI	5.8±1.88 mm	5.95±1.97 mm	0.8072
	p-value	<0.05	0.2671	
12	PI	11.88±2.04 mm	11.93±2.12 mm	0.8820
	SI	9.89±1.06 mm	9.75±0.74 mm	0.741
	p-value	<0.05	<0.05	

Table 3. Mean (± standard deviation) of bone area (mm² and%) of implants according to ROI.

weeks	ROI	PI (mm ²)	SI (mm ²)	p-value
4	1 (SI+PI) (peri-implant)	8.41 (±1.83) [40.56% (±8.83)]	8.10 (±1.35) [39.06% (±6.51)]	0.8860
	4-6 (PI) (intraporous)	0.84 (±0.22)		
	1 (SI)	9.25 (±1.95)	8.10 (±1.35)	<0.05
	1+4-6 (PI) (total)			
12	1 (SI+PI) (peri-implant)	7.32 (±1.49) [35.30% (±7.19)]	7.13 (±1.27) [34.39% (±6.12)]	0.9006
	4-6 (PI) (intraporous)	0.98 (±0.20)		
	1 (SI)+	8.30 (±1.52)	7.13 (±1.27)	<0.05
	1+4-6 (PI) (total)			

Table 4. Mean (± standard deviation) of bone area of implants according to ROI with p-value in time elapse (4 to 12 weeks).

ROI	weeks	PI (mm ²)	p-value SI in time elapse	SI (mm ²)	p-value PI in time elapse
1 (peri-implant)	4	8.41 (±1.83)	0.1456	8.10 (±1.35)	0.0831
	12	7.32 (±1.49)		7.13 (±1.27)	
4-6 (PI) (intraporous)	4	0.84 (±0.22)	0.4484		
	12	0.98 (±0.20)			
1 + 4-6 (total)	4	9.25 (±1.95)	0.1140	8.10 (±1.35)	0.0831
	12	8.30 (±1.52)		7.13 (±1.27)	

Table 5 Mean (± standard deviation) of peri-implant bone area (%) next to implant (ROI 3) and farther from implant (ROI 2) in time.

ROI	Implant	4 weeks (%)	12 weeks (%)	p-value
2	PI	37.12 (±11.57)	30.53 (±8.35)	0.0997
	SI	39.58 (±15.83)	27.13 (±9.02)	
	p-value	0.2110	0.0916	<0.05
3	PI	41.31 (±11.67)	39.19 (±10.3)	0.6271
	SI	39.27 (±15.02)	41.02 (±10.65)	
	p-value	0.6577	0.4424	0.7088

Table 6. Mean (± standard deviation) of intraporous bone area (%) of PI in time.

ROI	4 weeks (%)	p-value	12 weeks (%)	p-value	p-value
4	29.91 (±9.45)	<0.05	34.99 (±10.16)	<0.05	0.3450
5	17.89 (±5.18)		18.51 (±11.58)		0.9828
6	16.11 (±5.86)	0.6372	18.09 (±12.75)	0.926	0.6520

Histomorphometry of osseointegration of novel 3D porous Ti-6Al-4V titanium implants

Table 7. Mean (\pm standard deviation) of peri-implant bone area (%) (ROI 1) of cortical region (section 1-2) and trabecular region (section 3-4) separately for implant and time.

weeks	section	PI (%)	SI (%)	p-value	p.Holm
4	1	50.04 (± 6.26)	47.97 (± 8.4)	0.2860	0.8580
	2	44.96 (± 9.3)	41.44 (± 16.79)	0.3373	0.8580
	3	30.79 (± 8.4)	35.87 (± 15.8)	0.4462	0.3010
	4	32.84 (± 11.94)	35.35 (± 15.26)	0.1244	0.4976
12	1	40.04 (± 7.4)	41.69 (± 6.12)	0.0755	0.3775
	2	36.78 (± 10.08)	38.48 (± 9.54)	0.6179	1.0000
	3	30.56 (± 8.56)	30.13 (± 7.06)	0.8746	1.0000
	4	30.25 (± 7.88)	31.27 (± 8.86)	0.3096	1.0000

newly formed bone area peri-implant (ROI 1) clearly decreased from the cortical sections (1 + 2) to the trabecular sections (3 + 4) (Table 7). There is no statistically significant difference between the implant types in the individual adjacent sections (Table 7).

Discussion

The porous and solid Ti-6Al-4V test implants presented here were previously submitted to a comparative biomechanical push-out study using an animal model to investigate the osseous integration ability (Frosch et al., 2020). The PI showed a significantly stronger osseous anchoring strength compared to the SI both 4 and 12 weeks after implantation. Despite the presented optimized biomechanical push-out arrangements, the material composition, shape and size of the implants and test parameters often vary and therefore have a negative impact on the reliability and comparability of the biomechanical results. However, histomorphometric analyzes provide precise and reliable data for osseointegration that can substantiate biomechanical results and facilitate comparison with other studies. In order to evaluate the short-term osseointegration as well as the mid-term osseoremodeling, observation periods of 4 and 12 weeks were chosen. In this way, short-term osseointegration disorders and mid-term osseoremodeling disorders due to stress-shielding or load-transfer failure can be identified separately (Mouzin et al., 2001; Borsari et al., 2009). A three-dimensional representation of the peri-implant bone area is histomorphometrically not possible and the 3D micro-CT use is limited in characterization of bone response close to the surface due to metal artifacts (Stoppie et al., 2007). In order to get at least a three-dimensional impression, we have optimized the manufacturing process of the thin-ground preparations (iso-axial cutting) to create 4 sections along the longitudinal axis of the implant in combination with a total of 6 different ROIs along the axial axis of the implants.

The peri-implant bone area is obviously a critical area for osseous stabilization of the implants and it can be assessed very well and precisely calculated

histomorphometrically (Liu et al., 2012). After 4 and 12 weeks of follow-up, the newly formed bone area around the outside of the implants (ROI 1) did not reveal any significant differences between SI and PI. However, including the intraporous bone area (ROI 4-6), the total bone area of PI is significantly larger compared to SI. Accordingly, the intraporous bone fraction appears to be a key factor in the superior osseous anchoring strength of PI demonstrated in the previous biomechanical study (Frosch et al., 2020). Our values of bone area partly agree with the literature, although the reported values vary considerably (Cohen et al., 2017; Kuroshima et al., 2017; do Prado et al., 2018; Brogini et al., 2020; Lee et al., 2020). Some of the values found in the literature are higher than ours because the studies used the diaphyseal region with its strong cortex as an implantation site in contrast to our selected metaphyseal implantation site (Kuroshima et al., 2017; Lee et al., 2020). We chose the lateral femoral condyle because the metaphyseal implantation site enables the examination of partial cortical and trabecular bone and provides more clinically relevant information than the diaphyseal or medullary placement alone (Sumner et al., 2001). In the metaphyseal region there is a predominant hypodense trabecular structure and a less pronounced cortex, and it is expected that the bone area will be less than diaphyseal. Accordingly, we determined a considerably reduced trabecular bone area compared to the cortical region at 4 and 12 weeks, which was significant in most cases. Furthermore, the total bone area (trabecular and cortical region combined) decreased from 4 to 12 weeks. Chen et al. and He et al. support these findings as they consistently report a peak of bone remodeling at 6 weeks with a decrease of bone area in a rabbit and rat model, respectively (Chen et al., 2015; He et al., 2017). Whether this marginal bone loss is related to immunological reasons in the sense of a foreign body reaction or to biomechanical remodeling processes remains unclear on the basis of the histological images (Albrektsson et al., 2018).

In order to assess the peri-implant bone distribution more precisely, we have divided peri-implant ROI 1 (0 to +1000 μm) into a near-surface ROI 3 (0 to +500 μm) and a more distant ROI 2 (+500 to +1000 μm). After 4 weeks, the percentage distribution of the newly formed woven bone around the implant surface was still balanced between ROI 3 and ROI 2. After 12 weeks, however, the initially balanced ratio shifted in favor of ROI 3. In detail, the bone area further away from the surface (ROI 2) decreases significantly for SI and not significantly for PI from 4 to 12 weeks, while the bone area of ROI 3 remained similar for SI and PI. Accordingly, the newly formed lamellar bone has accumulated directly around the implant surface (0 to +500 μm) after the remodeling. Furthermore, there is also an accumulation of newly formed bone in the pores of ROI 4 near the surface (0 to -500 μm), which is even more pronounced in the course of remodeling after 12 weeks. Apparently, the crucial osseous fixation of the

implants appears to be within a radius of $\pm 500 \mu\text{m}$ around the surface. The results can be interpreted as a remodeling process with a functional restructuring and integration of the implant into the surrounding area. Tarala et al. confirm our results by reporting that a bone ingrowth depth of $500 \mu\text{m}$ into PI already resulted in a distinct interface strength and that a deeper ingrowth ($> 500 \mu\text{m}$) did not improve the interface strength considerably (Tarala et al., 2011).

Upon further examination of the intraporous region, a relevant portion of the mineralized bone was also detectable in the deeper pores of ROI 5 and 6 after 4 and 12 weeks. These findings correlate quite accurately with the results of Tarala et al., who reported a plateau of bone ingrowth reached at $1500 \mu\text{m}$ in porous titanium implants (Tarala et al., 2011). The evidence of mineralized bone in the pores even after mid-term osseoremodeling confirms the open porosity of PI and indicates a functional load transfer and thus an intact continuous mechanotransduction into the pores. Mechanotransduction is a conversion of mechanical stimuli (functional stress) into electrochemical activity and a basic requirement for permanent new bone formation as part of the remodeling and repair processes (Wolff, 1892; Allori et al., 2008). We therefore assume that the mineralized intraporous bone area contributes considerably to the functional load transfer from the surrounding bone to the implant (and vice versa), resulting in a stronger osseous anchoring of the PI compared to the SI.

The 3D porosity of the material is essential for deeper bone ingrowth. Kuboki et al. demonstrated neovascularity and a penetration of mesenchymal cells into PI as a basic condition for intraporous osteogenesis (Kuboki et al., 1998). In addition to the indirect evidence of a stable vascularization in form of mineralized bone, we were also able to histologically demonstrate vessels as well as osteoblasts and osteoclast in the deep pores of PI after 12 weeks. We conclude that the open porosity of the sintered implant further improves the osseous integration.

The qualitative histological assessment showed a regular development of mineralized woven bone after 4 weeks of osseohaling and lamellar bone after 12 weeks of osseoremodeling but without any substantial difference between SI and PI. According to Branemark et al. and Albrektsson et al., there should be a direct BIC without interposing soft tissue at the resolution level of light microscope in order to meet the criteria of osseointegration (Branemark et al., 1977; Albrektsson et al., 1981). This definition is still relevant despite further development of the term osseointegration (Albrektsson and Wennerberg, 2019). The BIC is usually given in percentage points. When two implants with the same surface properties are compared, the BIC can provide a good conclusion and comparison about the bony integration. The higher the BIC, the better the bony anchoring of implants of the same size usually is (Wennerberg et al., 1995). In the present case, the percentage of BIC is similar when comparing the

implant types, without any significant difference after 4 or 12 weeks. These findings indicate similar osteoconductive and osteoinductive properties of both implant types. However, the two types of implants have different surface properties and the outer porous recesses of PI functionally enlarge the implant circumference significantly compared to SI. Based on the percentage of BIC and the different implant circumferences of PI and SI, the actual bony contact in mm to the outer implant circumference was significantly larger to PI than to SI. We assume that the larger osseous contact of PI is a crucial factor for the superior biomechanical anchoring strength of PI compared to SI as previously shown (Frosch et al., 2020).

The BIC of both implant types increased significantly from 4 to 12 weeks during remodeling. These results are in agreement with the results found in the literature and the results of our previous biomechanical study, which also showed an increase in bone fixation from 4 to 12 weeks (Cohen et al., 2016; Brizuela-Velasco et al., 2017; Brogini et al., 2020; Frosch et al., 2020).

The presented results of BIC underline the functional importance and its role as a key indicator for osseointegration (Bernhardt et al., 2012; Gahlert et al., 2012). Our BIC results range between the values given in the literature, which vary roughly between 20% and 68% for Ti-6Al-4V implants (Cohen et al., 2016, 2017; Brizuela-Velasco et al., 2017; Kuroshima et al., 2017; do Prado et al., 2018; Brogini et al., 2020). In our opinion, the histologic differentiation and evaluation of the BIC is not always trivial and the histologic measurement accuracy depends not only on interobserver reliability, but also on the quality of the selected histological staining, the thin-ground process, and the further image digitalization. Even with supposedly direct BIC in the light microscopic overview image, osseointegrated implants often reveal thin soft tissue layers at the interface at higher magnification (Liu et al., 2012). To our knowledge, there is no general definition of how much bone-to-implant distance is considered as a direct BIC. An approach might be to regard it as contact if nothing is between bone and implant even if there is a distance less than $10 \mu\text{m}$ and bone is following the implant shape perfectly. The interposition of collagen layers within the $10 \mu\text{m}$ should possibly be accepted, while tissue containing cell bodies or traces of stains should be considered more critically when assessing whether or not a direct BIC is present. In our impression, we tended to use rather strict criteria when defining the BIC, which does not have a negative effect on the comparison within the study, but may lead to comparably lower values.

Funding. This project was supported by the Federal Ministry for Science and Technology of Germany (BMWWT – ZIM - KA 2002 23 02 MD 8).

Data availability statement. The datasets generated during and/or analyzed during the current study are available from the corresponding author on reasonable request.

Histomorphometry of osseointegration of novel 3D porous Ti-6Al-4V titanium implants

References

- Albrektsson T. and Wennerberg A. (2019). On osseointegration in relation to implant surfaces. *Clin. Implant. Dent. Relat. Res.* 21 Suppl. 1, 4-7.
- Albrektsson T., Branemark P.I., Hansson H.A. and Lindstrom J. (1981). Osseointegrated titanium implants. Requirements for ensuring a long-lasting, direct bone-to-implant anchorage in man. *Acta. Orthop. Scand.* 52, 155-170.
- Albrektsson T., Chrcanovic B., Mölne J. and Wennerberg A. (2018). Foreign body reactions, marginal bone loss and allergies in relation to titanium implants. *Eur. J. Oral Implantol.* 11 (Suppl. 1), S37-S46.
- Allori A.C., Sailon A.M., Pan J.H. and Warren S.M. (2008). Biological basis of bone formation, remodeling, and repair-part III: Biomechanical forces. *Tissue Eng. Part B Rev.* 14, 285-293.
- Bencharit S., Byrd W.C., Altarawneh S., Hosseini B., Leong A., Reside G., Morelli T. and Offenbacher S. (2014). Development and applications of porous tantalum trabecular metal-enhanced titanium dental implants. *Clin. Implant Dent. Relat. Res.* 16, 817-826.
- Bernhardt R., Kuhlisch E., Schulz M.C., Eckelt U. and Stadlinger B. (2012). Comparison of bone-implant contact and bone-implant volume between 2D-histological sections and 3D-sr-microct slices. *Eur. Cell. Mater.* 23, 237-247.
- Bobyn J.D., Pilliar R.M., Cameron H.U. and Weatherly G.C. (1980). The optimum pore size for the fixation of porous-surfaced metal implants by the ingrowth of bone. *Clin. Orthop. Relat. Res.* 150, 263-270.
- Borsari V., Fini M., Giavaresi G., Tschon M., Chiesa R., Chiusoli L., Salito A., Rimondini L. and Giardino R. (2009). Comparative in vivo evaluation of porous and dense duplex titanium and hydroxyapatite coating with high roughnesses in different implantation environments. *J. Biomed. Mater. Res. A* 89, 550-560.
- Bram M. (2013). Pulvermetallurgische herstellung von porösem titan und von niti-legierungen für biomedizinische anwendungen. *Schriften des Forschungszentrums Jülich*
- Bram M., Laptev A., Buchkremer H.P. and Stoever D. (2004). Near-net-shape manufacturing of highly porous titanium parts for biomedical applications. *Mat.-wiss. u. Werkstofftechnik* 35/4, Wiley-VCH, Weinheim.
- Branemark P.I., Hansson B.O., Adell R., Breine U., Lindstrom J., Hallen O. and Ohman A. (1977). Osseointegrated implants in the treatment of the edentulous jaw. Experience from a 10-year period. *Scand. J. Plast. Reconstr. Surg. (Suppl 16)*, 1-132.
- Brizuela-Velasco A., Perez-Pevida E., Jimenez-Garrudo A., Gil-Mur F.J., Manero J.M., Punset-Fuste M., Chavarri-Prado D., Dieguez-Pereira M. and Monticelli F. (2017). Mechanical characterisation and biomechanical and biological behaviours of ti-zr binary-alloy dental implants. *Biomed. Res. Int.* 2017, 2785863.
- Brogini S., Sartori M., Giavaresi G., Cremascoli P., Alemani F., Bellini D., Martini L., Maglio M., Pagani S. and Fini M. (2020). Osseointegration of additive manufacturing ti-6al-4v and co-cr-mo alloys, with and without surface functionalization with hydroxyapatite and type i collagen. *J. Mech. Behav. Biomed. Mater.* 115, 104262.
- Chen W.T., Han da C., Zhang P.X., Han N., Kou Y.H., Yin X.F. and Jiang B.G. (2015). A special healing pattern in stable metaphyseal fractures. *Acta. Orthop.* 86, 238-242.
- Cohen D.J., Cheng A., Sahingur K., Clohessy R.M., Hopkins L.B., Boyan B.D. and Schwartz Z. (2017). Performance of laser sintered ti-6al-4v implants with bone-inspired porosity and micro/nanoscale surface roughness in the rabbit femur. *Biomed. Mater.* 12, 025021.
- Cohen D.J., Cheng A., Kahn A., Aviram M., Whitehead A.J., Hyzy S.L., Clohessy R.M., Boyan B.D. and Schwartz Z. (2016). Novel osteogenic Ti-6Al-4V device for restoration of dental function in patients with large bone deficiencies: Design, development and implementation. *Sci. Rep.* 6, 20493.
- Dahl L.K. (1952). A simple and sensitive histochemical method for calcium. *Proc. Soc. Exp. Biol. Med.* 80, 474-479.
- do Prado R.F., Esteves G.C., Santos E.L.S., Bueno D.A.G., Cairo C.A.A., Vasconcellos L.G.O., Sagnori R.S., Tessarin F.B.P., Oliveira F.E., Oliveira L.D., Villaca-Carvalho M.F.L., Henriques V.A.R., Carvalho Y.R. and De Vasconcellos L.M.R. (2018). In vitro and in vivo biological performance of porous ti alloys prepared by powder metallurgy. *PLoS One* 13, e0196169.
- Frosch K.H., Barvencik F., Lohmann C.H., Viereck V., Siggelkow H., Breme J., Dresing K. and Sturmer K.M. (2002). Migration, matrix production and lamellar bone formation of human osteoblast-like cells in porous titanium implants. *Cells Tissues Organs* 170, 214-227.
- Frosch K.H., Barvencik F., Viereck V., Lohmann C.H., Dresing K., Breme J., Brunner E. and Sturmer K.M. (2004). Growth behavior, matrix production, and gene expression of human osteoblasts in defined cylindrical titanium channels. *J. Biomed. Mater. Res. A* 68, 325-334.
- Frosch S., Nusse V., Frosch K.H., Lehmann W. and Buchhorn G. (2020). Osseointegration of 3D porous and solid ti-6al-4v implants - narrow gap push-out testing and experimental setup considerations. *J. Mech. Behav. Biomed. Mater.* 115, 104282.
- Gahlert M., Roehling S., Sprecher C.M., Kniha H., Milz S. and Bormann K. (2012). In vivo performance of zirconia and titanium implants: A histomorphometric study in mini pig maxillae. *Clin. Oral. Implants Res.* 23, 281-286.
- Gittens R.A., Scheideler L., Rupp F., Hyzy S.L., Geis-Gerstorfer J., Schwartz Z. and Boyan B.D. (2014). A review on the wettability of dental implant surfaces ii: Biological and clinical aspects. *Acta Biomater.* 10, 2907-2918.
- Hartmann M. (2012). Ein beitrag zur zellulären bauweise von implantatwerkstoffen nach dem vorbild der natur. *Faculty of Natural Sciences and Technology III C, Pharmacy, bio and materials science, Saarland University.*
- He T., Cao C., Xu Z., Li G., Cao H., Liu X., Zhang C. and Dong Y. (2017). A comparison of micro-CT and histomorphometry for evaluation of osseointegration of peo-coated titanium implants in a rat model. *Sci. Rep.* 7, 16270.
- Itala A.I., Ylanen H.O., Ekholm C., Karlsson K.H. and Aro H.T. (2001). Pore diameter of more than 100 microm is not requisite for bone ingrowth in rabbits. *J. Biomed. Mater. Res.* 58, 679-683.
- Jones A.C., Arns C.H., Sheppard A.P., Hutmacher D.W., Milthorpe B.K. and Knackstedt M.A. (2007). Assessment of bone ingrowth into porous biomaterials using micro-CT. *Biomaterials* 28, 2491-2504.
- Karageorgiou V. and Kaplan D. (2005). Porosity of 3D biomaterial scaffolds and osteogenesis. *Biomaterials* 26, 5474-5491.
- Kawebulum M., Aguilar M.C., Blancas E., Kawebulum J., Lehman W.B., Grant A.D. and Strongwater A.M. (1994). Histological and radiographic determination of the age of physeal closure of the distal femur, proximal tibia, and proximal fibula of the new zealand white rabbit. *J. Orthop. Res.* 12, 747-749.
- Kim D.G., Huja S.S., Tee B.C., Larsen P.E., Kennedy K.S., Chien H.H., Lee J.W. and Wen H.B. (2013). Bone ingrowth and initial stability of titanium and porous tantalum dental implants: A pilot canine study.

Histomorphometry of osseointegration of novel 3D porous Ti-6Al-4V titanium implants

- Implant. Dent. 22, 399-405.
- Kuboki Y., Takita H., Kobayashi D., Tsuruga E., Inoue M., Murata M., Nagai N., Dohi Y. and Ohgushi H. (1998). BMP-induced osteogenesis on the surface of hydroxyapatite with geometrically feasible and nonfeasible structures: Topology of osteogenesis. *J. Biomed. Mater. Res.* 39, 190-199.
- Kuroshima S., Nakano T., Ishimoto T., Sasaki M., Inoue M., Yasutake M. and Sawase T. (2017). Optimally oriented grooves on dental implants improve bone quality around implants under repetitive mechanical loading. *Acta Biomater.* 48, 433-444.
- Lee S., Chang Y.Y., Lee J., Madhurakkat Perikamana S.K., Kim E.M., Jung Y.H., Yun J.H. and Shin H. (2020). Surface engineering of titanium alloy using metal-polyphenol network coating with magnesium ions for improved osseointegration. *Biomater. Sci.* 8, 3404-3417.
- Liu S., Broucek J., Virdi A.S. and Sumner D.R. (2012). Limitations of using micro-computed tomography to predict bone-implant contact and mechanical fixation. *J. Microsc.* 245, 34-42.
- Masoud I., Shapiro F., Kent R. and Moses A. (1986). A longitudinal study of the growth of the new zealand white rabbit: Cumulative and biweekly incremental growth rates for body length, body weight, femoral length, and tibial length. *J. Orthop. Res.* 4, 221-231.
- Moreira C.A. and Dempster D.W. (2020). Chapter 19 - histomorphometric analysis of bone remodeling. Academic Press.
- Mouzin O., Soballe K. and Bechtold J.E. (2001). Loading improves anchorage of hydroxyapatite implants more than titanium implants. *J. Biomed. Mater. Res.* 58, 61-68.
- Rausch G., Hartwig T., Weber M. and Schulz O. (2000). Herstellung und eigenschaften von titanschäumen [production and characteristics of titanium foam]. *Mat.-wiss. u. Werkstofftechnik* 31, 412-414.
- Rosa A.L., Crippa G.E., de Oliveira P.T., Taba M., Jr., Lefebvre L.P. and Beloti M.M. (2009). Human alveolar bone cell proliferation, expression of osteoblastic phenotype, and matrix mineralization on porous titanium produced by powder metallurgy. *Clin. Oral Implants Res.* 20, 472-481.
- Smith L.G. and Karagianes M.T. (1974). Histological preparation of bone to study ingrowth into implanted materials. *Calcif. Tissue Res.* 14, 333-337.
- Stoppie N., Wevers M. and Naert I. (2007). Feasibility of detecting trabecular bone around percutaneous titanium implants in rabbits by in vivo microfocus computed tomography. *J. Microsc.* 228, 55-61.
- Sumner D.R., Turner T.M. and Urban R.M. (2001). Animal models relevant to cementless joint replacement. *J. Musculoskelet. Neuronal. Interact.* 1, 333-345.
- Sumner D.R., Turner T.M., Igloria R., Urban R.M. and Galante J.O. (1998). Functional adaptation and ingrowth of bone vary as a function of hip implant stiffness. *J. Biomech.* 31, 909-917.
- Tarala M., Waanders D., Biemond J.E., Hannink G., Janssen D., Buma P. and Verdonshot N. (2011). The effect of bone ingrowth depth on the tensile and shear strength of the implant-bone e-beam produced interface. *J. Mater. Sci. Mater. Med.* 22, 2339-2346.
- Vasconcellos L.M., Leite D.O., Oliveira F.N., Carvalho Y.R. and Cairo C.A. (2010). Evaluation of bone ingrowth into porous titanium implant: Histomorphometric analysis in rabbits. *Braz. Oral Res.* 24, 399-405.
- Wennerberg A., Albrektsson T. and Chrcanovic B. (2018). Long-term clinical outcome of implants with different surface modifications. *Eur. J. Oral Implantol.* 11 (Suppl 1), S123-S136.
- Wennerberg A., Albrektsson T., Andersson B. and Krol J.J. (1995). A histomorphometric and removal torque study of screw-shaped titanium implants with three different surface topographies. *Clin. Oral Implants Res.* 6, 24-30.
- Wolff J. (1892). *Das gesetz der transformation der knochen*. Hirschwald, Berlin.
- Xue W., Krishna B.V., Bandyopadhyay A. and Bose S. (2007). Processing and biocompatibility evaluation of laser processed porous titanium. *Acta Biomater.* 3, 1007-1018.

Accepted May 11, 2021